

Closed Loop Control of Halbach Array Magnetic Levitation System Height

(CLCML)

Senior Project Final Report

Students:

Kyle Gavelek

Victor Panek

Christopher Smith

Advisors:

Dr. Winfred Anakwa

Mr. Steven Gutschlag

Date:

May 16, 2013

abstract – Magnetic levitation systems are used in magnetic levitation trains and industrial rotating machinery applications. Magnetic levitation trains can travel at very high speed because there is no contact friction. Dr. Richard Post pioneered an alternative approach, the Halbach array-inductrack method, which requires no external energy for levitation. Previous years' projects at Bradley University demonstrated this method using a rotary inductrack with a Halbach array of magnets. The goal of the project is design of controller to achieve closed loop control of magnetic levitation system height. A model of the DC motor driving the inductrack rotary wheel was determined experimentally, and the levitation force was measured. An optical encoder was used to sense the rotary wheel velocity which was compared to desired velocity related to a desired levitation height. The velocity error is sent to a controller implemented on 8051 microcontroller which generated a pulse width modulated signal to drive the motor. The microcontroller also displayed the levitation height sensed by a linear position sensor.

Table of Contents

Background	3
Magnetic Levitation	3
Halbach Array - Inductrack Theory	3
CLCML Project	7
Current Halbach Array - Inductrack System.....	7
Project Objective.....	9
Planning	10
Lookup Table.....	11
Controller	11
DC Motor Modeling	11
Design.....	11
Motor Modeling.....	11
Controller Design	23
Halbach Array Data Collection	27
Microcontroller Implementation	31
Results.....	31
Patents	33
References	34

Background

Magnetic Levitation

Magnetic levitation has been used in commercial transportation maglev trains since 1984. By using magnetic levitation instead of traditional methods, these high-speed trains can nearly eliminate frictional costs. Currently, there are two different methods of maglev in operation – electromagnetic suspension and electrodynamic suspension. However, both of these methods require power to activate the magnetic levitation. The inductrack method allows for magnetic levitation to occur from a completely passive system, in turn creating the potential for an even more efficient method of transportation. The inductrack maglev system creates magnetic levitation through the interaction of the inductrack and magnets. The inductrack method was developed by Dr. Richard Post in the late 1990's at Lawrence Livermore National Laboratory. His inductrack team formulated the governing equations of the Halbach array-inductrack relationship.

Halbach Array - Inductrack Theory

Halbach Array of Magnets

The Halbach array was designed by Klaus Halbach for use with particle accelerators. A Halbach Array is a specific orientation of magnets designed to direct each magnet's field below the array while nearly cancelling the magnetic field above the array. Shown in Figure 1 are the magnetic fields generated by a Halbach array of magnets, which results in a sinusoidal magnetic field. The wavelength of this field can be calculated based on the length of the magnet array, as shown in Figure 2. The wavelength λ of the sinusoidal magnetic field is measured as the distance between the midway points of each end magnet. If the magnets are all the same length, λ is equal to the total length of the magnet array minus the length of one magnet.

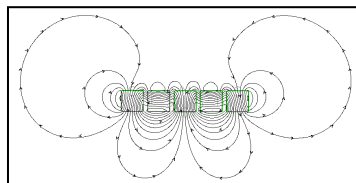


Fig. 1. Halbach Array Magnetic Field

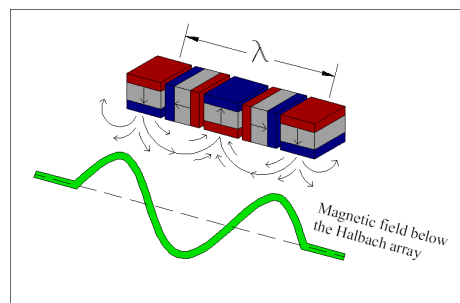


Fig. 2. Sinusoidal Magnetic Field

The peak magnetic field of the sinusoidal field generated by the magnetic Halbach array can be calculated by equation (1):

$$B_0 = \frac{B_r(1-e^{-kd})\sin(\pi/M)}{\pi/M} \quad [\text{Tesla}] \quad (1)$$

B_0 – peak magnetic field
 B_r – individual magnet’s strength
 k – wavenumber
 M – number of magnets per wavelength

Inductrack

The inductrack is an array of inductors designed to interact with a Halbach Array of magnets to produce magnetic levitation. Dr. Post’s inductrack team found that when the inductrack rotates underneath the Halbach Array device, the changing magnetic field induces a magnetic flux relationship of equation (2):

$$\Phi(t) = \frac{B_0 w}{k} e^{-ky} \sin(\omega_e t) (1 - e^{-ky}) \quad [\text{Weber}] \quad (2)$$

w – width of the inductrack
 ω_e – excitation frequency
 y – vertical displacement

This induced magnetic flux generates a current and a voltage in each circuit along the inductrack given by equations (3) and (4):

$$i(t) = \frac{\Phi_0}{L} \left[\frac{1}{1 + \left(\frac{R}{\omega_e L}\right)^2} \right] [\sin(\omega_e t) + \frac{R}{\omega_e L} \cos(\omega_e t)] \quad [\text{Amps}] \quad (3)$$

$$v(t) = \omega_e \Phi_0 \cos(\omega_e t) \quad [\text{Volts}] \quad (4)$$

Φ_0 – peak magnetic flux
 ω_e – excitation frequency
 R – track resistance
 L – track inductance

The peak magnetic flux is calculated from Equation (2) in the following equation:

$$\Phi_0 = \frac{B_0 w}{k} e^{-ky} \quad [\text{Weber}] \quad (5)$$

The Halbach array-inductrack system can be modeled as a simple RL circuit as shown in Figure 3. Note that $v(t)$ defined by equation (4) above represents the voltage induced by the passing Halbach array device, while resistance and inductance represent the passive inductrack properties. As the frequency of $v(t)$ increases, which is equivalent to the array’s velocity, phase lag will increase. The phase lag of the voltage causes the magnetic field generated by the inductrack to lag and eventually align itself with the Halbach Array’s magnetic field.

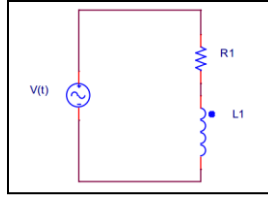


Fig. 3. RL Circuit Model for Halbach array-Inductrack System

This phenomenon can be observed in the series of pictures in Figure 4. The dial on the right side represents velocity so that the pictures from top to bottom represent increasing velocity. Observe that, as velocity increases, the induced magnetic field lag increases. At high velocity, lowest picture, the induced magnetic field lag reaches a maximum where the like magnetic poles align, causing maximum vertical magnetic repulsion.

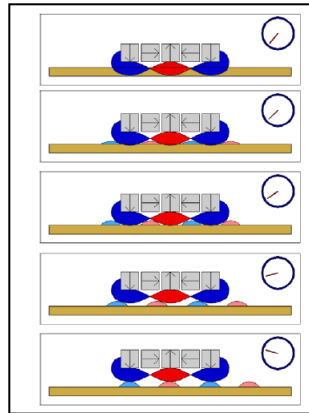


Fig. 4. Phase Lag-Velocity Relationship. Velocity increases from top depiction to bottom depiction.

Another way to view this relationship is shown in Figure 5, the Bode phase plot for a series RL circuit. The pole will occur at $-R/L$, which corresponds to a phase lag of 45 degrees. At high frequency, phase lag approaches 90 degrees.

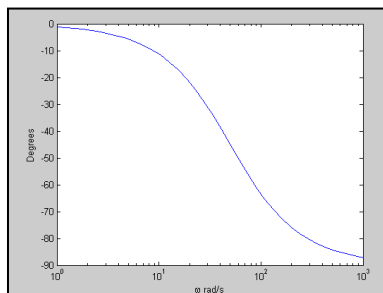


Fig. 5. Bode Phase Plot of a Series RL Circuit

The force produced by the Halbach Array-inductrack system can be broken into lift and drag force shown by equations (6) and (7):

$$F_y(\omega_e, y) = \frac{B_0^2 w A}{2kLd_c} \left[\frac{1}{1 + \left(\frac{R}{\omega_e L}\right)^2} \right] e^{-2ky} \quad [\text{Newton}] \quad (6)$$

$$F_x(\omega_e, y) = \frac{B_0^2 w A}{2kLd_c} \left[\frac{R/\omega_e L}{1 + \left(\frac{R}{\omega_e L}\right)^2} \right] e^{-2ky} \quad [\text{Newton}] \quad (7)$$

d_c – center spacing of the conducting strips

A – area under Halbach array

The remaining parameters in this relationship are defined above. Due to the fact that all but excitation frequency, ω_e , and vertical displacement, y , are constant, the force, F_y , is expressed as a function of these two variables. Therefore, breakpoint excitation frequency can be solved for a known mass and initial displacement. This relationship can be rearranged to solve for displacement, y , as a function of excitation frequency, ω_e , given by equation (6):

$$y(\omega_e) = \frac{1}{2k} \ln \left(\frac{B_0^2 w A}{2kLd_c F \left[1 + \left(\frac{R}{\omega_e L}\right)^2 \right]} \right) \quad [\text{meter}] \quad (8)$$

F – vertical force experienced by the Halbach array

In equation (8), the vertical force F experienced is assumed to be constant, simply the force required to levitate the mass, and thus only displacement y will vary with changing excitation frequency.

The excitation frequency has a direct relationship to the linear velocity of the Halbach array shown in equation (9):

$$\omega_e = kv \quad [\text{rad/s}] \quad (9)$$

v – linear velocity in meters per second

It should be noted that in rotational systems, linear velocity is denoted as tangential velocity v_t . In rotational systems, excitation frequency can be expressed as function of rotational velocity ω_m shown in equation (8):

$$\omega_e = kr\omega_m \quad [\text{rad/s}] \quad (9)$$

r – radius of motion

ω_m – rotational velocity

It is important to not confuse ω_m and ω_e . Both variables have units of radians per second, but ω_e is an electrical frequency while ω_m is a mechanical frequency.

CLCML Project

Current Halbach Array - Inductrack System

Dr. Post's work is the foundation of Paul Friend's research compiled for his 2003-2004 Senior Capstone Project at Bradley University. Mr. Friend designed and implemented the first magnetic levitation system at Bradley University. Mr. Friend also created a MATLAB Graphical User Interface to simulate the Halbach Array - inductrack graphical relationships while customizing inductrack methods and parameters. Using Mr. Friend's research, Glenn Zomchek designed a magnetic levitation system using the rotary inductrack method for his 2006-2007 Senior Capstone Project. Mr. Zomchek obtained successful levitation of 0.45 millimeters. Building on Mr. Zomchek's system, Dirk DeDecker and Jesse Vanlsegheem redesigned the magnetic levitation system to have a larger rotary inductrack wheel for their 2011-2012 Senior Capstone Project. The DeDecker-Vanlsegheem rotary inductrack system shown in Figure 6 achieved 3.7 millimeters of vertical displacement. The previous years' research and labor provides a foundation for this year's CLCML Senior Capstone Project.

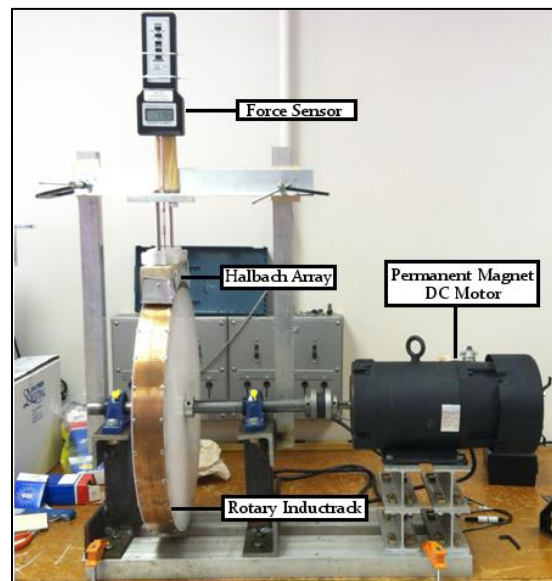


Fig. 6. DeDecker-Vanlsegheem Inductrack System

Halbach Array Parameters

The magnetic Halbach array used in the current system is shown in Figure 7. It was designed to fit the curvature of the rotary wheel driven by the DC motor. The top portion was designed and fabricated to allow it to be attached to a metal bracket that can be attached so that the Halbach array is suspended at an adjustable height. Altogether, the mass of the levitation array and its housing is 4.65 kilograms.

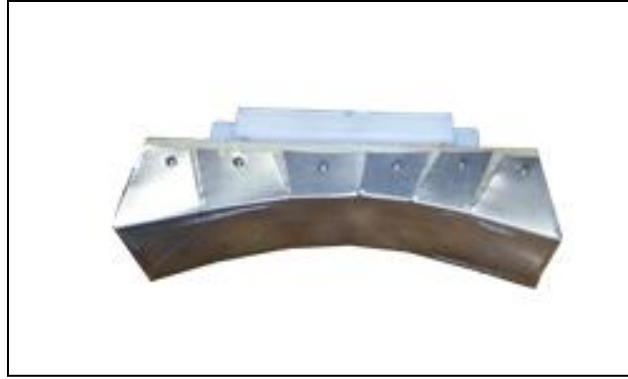


Fig. 7. DeDecker-Vanlsegghem Designed Halbach Array Device

Mr. DeDecker and Mr. Vanlsegghem calculated the peak magnetic field strength of this Halbach Array based on the following parameters:

$$k = 224.4 \text{ rad/meter}$$

$$d = 0.006 \text{ meter}$$

$$B_r = 1.21 \text{ Tesla}$$

$$M = 4 \text{ magnets/wavelength}$$

Using Equation (1) yields

$$B_0 = 0.8060 \text{ [T]}$$

Inductrack Parameters

The copper track shown in Figure 8 was fabricated by Mr. DeDecker and Mr. Vanlsegghem. It is screwed into place around the rotary wheel that is connected to the DC motor shaft. It was designed to maximize track inductance while minimizing track resistance. This design choice was intended to shift the pole frequency towards the origin so that phase lag, and thus magnetic repulsion, would occur at a lower velocity.

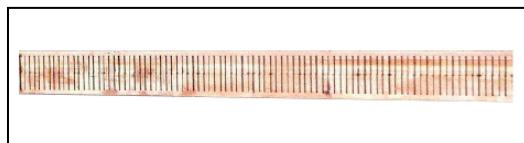


Fig. 8. Copper Inductrack

The track resistance and inductance can be determined using equations (10) and (11):

$$R = R_c \frac{l}{A} \quad [\text{Ohm}] \quad (10)$$

$$L = \mu_0 \frac{P_c}{2kd_c} \quad [\text{Henry}] \quad (11)$$

R_c = resistivity of copper

μ_0 = permeability of free space

l = length of the slot

P_c = mean perimeter of inductrack

A = crosssectional area of the inductrack

d_c = Spacing of inductors

Mr. DeDecker and Mr. Vanlseghem calculated the following inductrack properties:

$$R = 1.90 \times 10^{-4} \quad [\Omega]$$

$$L = 7.532 \times 10^{-8} \quad [\text{H}]$$

However, after simulations, they suspected that the calculated R and L did not match the actual track resistance and inductance. The track parameters were then recalculated.

$$l = 0.04 \text{ meters} \quad A = 3.175 \times 10^{-6} \text{ meters}^2 \quad R_c = 1.68 \times 10^{-8} \Omega \text{ meter}$$

Therefore,

$$R = 2.12 \times 10^{-4} \quad [\Omega]$$

And the track inductance was recalculated with the following measurements:

$$P_c = 0.098 \text{ meters} \quad d_c = 0.004 \text{ meters} \quad k = 224.4 \text{ rad/meter} \quad \mu_0 = 4\pi \times 10^{-7} \text{ Henry/meter}$$

Therefore,

$$L = 6.86 \times 10^{-8} \quad [\text{H}]$$

These calculations are only slightly different from last year's due slight differences in perimeter measurement. These updated values are used in all future calculations.

Project Objective

The objective of CLCML is to improve the 2011-2012 Senior Capstone Project's magnetic levitation system and implement closed loop control of the magnetic levitation height of the Halbach Array of magnets. In order to accomplish this objective, CLCML had the following goals:

- Improve the rotational stability of the inductrack by balancing the wheel

- Construct a safety enclosure in order to safely reach higher rotational velocities
- Model the DC motor and verify its accuracy to within +/- 5% of steady state rotational velocity
- Design a controller to achieve closed loop control of displacement height
- Implement the controller using a microcontroller

Planning

CLCML's objective is to achieve closed-loop control of the magnetic levitation height of the Halbach Array of magnets. Shown in Figure 9 is the top level system block diagram of the closed loop feedback.

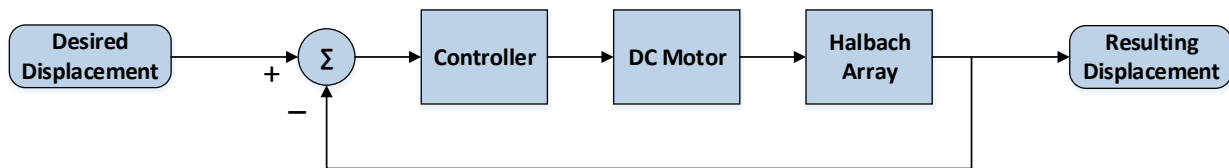


Fig. 9. High Level System Block Diagram

The input to the system is the desired displacement, while the output is the resulting displacement. The system uses negative feedback of the levitation height to create a displacement error as input to the controller. In order to achieve closed-loop control of the levitation height, models of the Halbach array-inductrack interaction and the DC motor will be created. However, it was decided due to the nonlinearity of the Halbach array model, a lookup table would be used to model this subsystem. As a result of this change, the system block diagram was rearranged.

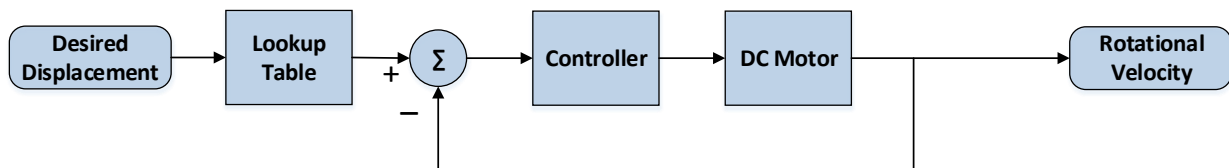


Fig. 10. High Level System Block Diagram with Lookup Table

The major difference with the rearranged block diagram in Figure (10) is that the controller is based solely on the motor model. Negative feedback is achieved in the form of rotational velocity as opposed to system height as in Figure (9). By controlling velocity, we achieve control of the levitation height.

Lookup Table

The Halbach array subsystem was created by using a lookup table based on experimental results. This subsystem's purpose is to convert the desired levitation displacement to rotational velocity of the inductrack. Therefore, an experiment was needed to measure displacement at a range of rotational velocities. The minimum increment of the user's displacement input would be determined after the experimental results were analyzed.

Controller

The controller was design to improve the system's response to an input. Due to the decision to use a lookup table for the Halbach array subsystem, the controller was design based solely upon the motor model. The controller was designed to meet the following specifications:

- The maximum overshoot of the system shall be less than 10%.
- The steady state error shall be 0.
- The settling time shall be minimized based on the other specifications.

The settling time specification had to be determined after motor modeling to determine the motor's capabilities. A reasonable settling time specification will be determined based on the motor response time to input voltage during motor modeling.

DC Motor Modeling

No datasheet could be found on the 20-year old motor, so an experiment was performed to derive the motor model. Motor modeling required a locked-rotor experiment as well as a coast-down experiment. The motor model's target accuracy was +/- 5% steady state rotational velocity from a range of 450-750 RPM. These speeds represent the range where we expect to find the breakpoint velocity. A tachometer would be used to compare experimental rotational speed to a simulation speed of the subsystem in Simulink at varying input voltages.

Design

Motor Modeling

In total, four separate motor models were derived, each one improving on the last by way of better methods. Here are the methods used in the final modeling experiment.

Shown in Figure (11) is a common schematic for DC motors.

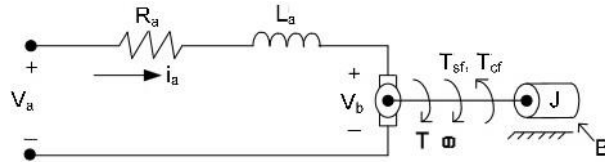


Fig. 11. DC Motor Circuit Schematic

Measurable quantities of DC motor circuit:

ω_m – machine rotational speed

i – amature current

V_a – source voltage

V_b – back emf voltage

Parameters to be determined of DC motor circuit:

R_a – armature resistance

L_a – armature inductance

k_v – motor torque constant

k_T – back emf constant

B – motor viscous friction coefficient

T_{cf} – coloumbic friction torque constant

J – moment of inertia

By analyzing the schematic, Equations (11), (12), (13) and (14) can be derived:

$$L_a \frac{di}{dt} + R_a i = V_a - V_b \quad (11)$$

$$V_b = k_v \omega_m \quad (12)$$

$$T = k_T I \quad (13)$$

$$J \frac{d\omega_m}{dt} = T - B\omega_m - T_{cf} \quad (14)$$

Equation (11) is found through Kirchhoff's Voltage Law – the sum of voltage around a loop must equal zero. Equation (12) introduces k_v , the Back emf Constant, which represents the ratio of voltage drop through the motor to rotational velocity of the motor shaft. In Equation (13), k_T is the Motor Torque Constant that represents the ratio of motor torque to armature current. Equation (14) is found through the Conservation of Energy for rotational systems. Also due to the Conservation of Energy, electrical power must equal (I think) mechanical power, thus k_v and k_T are equal. Using Equations (11)-(14), a system block diagram can be formed, which is shown in Figure (12).

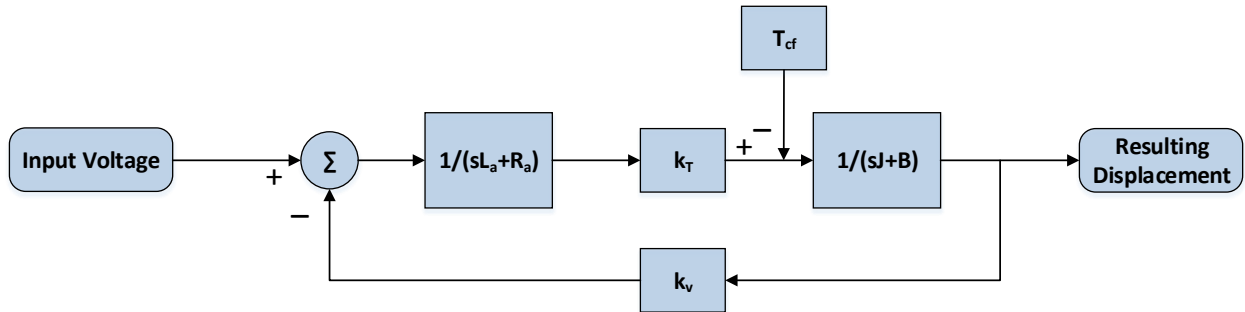


Fig. 12. Motor Model Subsystem

Determination of Armature Resistance

By analyzing the DC motor circuit in Figure (11), armature resistance R_a can be isolated. Substituting Equation (12) into (11):

$$L_a \frac{di}{dt} + R_a i = V_a - k_v \omega_m$$

When a DC voltage is input into the motor ($\frac{di}{dt} = 0$), and no shaft rotation is allowed ($\omega_m = 0$), the system is simplified to a resistive circuit.

$$R_a i = V_a$$

This experiment is called the locked rotor test. By recording the input voltage and measuring the armature current with a current probe, armature resistance can be determined. The rotor was held in place while entering a range of input voltages to record the resulting armature resistance.

V_a [V] <i>Digital Multimeter</i>	i [A] <i>Current Probe</i>	R_a [Ω] $R = V_a / I_a$
1.0	0.20	5.00
2.0	0.45	4.40
3.2	1.00	3.20
5.2	2.00	2.60
6.5	3.00	2.16
8.0	4.00	2.00
9.3	5.00	1.86
11.0	6.00	1.83

Table 1. Locked Rotor Experimental Results

Armature resistance is the brush resistance within the motor and variable based on current. Since we will be operating the motor with currents between 2 and 6 amps, $R_a = 2.0 [\Omega]$ was selected as an appropriate estimation of the bottom five measurements.

Determination of Armature Inductance

To determine armature inductance, the complete response of the system's current was observed to discover the electrical time constant τ_e . For RL circuits, $\tau_e = \frac{L_a}{R_a}$. When the system is relaxed, an input voltage was applied at time $t = 0$. The input voltage was selected so that no rotation of the rotor would occur. A knife switch was used in place of a traditional switch to eliminate switch bounce effects. The $i(t)$ curve was observed on an oscilloscope with a current probe.

$$i(\tau_e) \approx .632i_{ss}$$

$$L_a = R_a\tau_e$$

It was observed that τ_e occurred at approximately 10.8 milliseconds. Therefore, $L_a = 0.0216[H]$.

Determination of Back emf and Motor Torque Constants

When the a DC voltage ($\frac{di}{dt} = 0$), is input and the rotor is moving at an unchanging velocity Equation (13) simplifies:

$$R_a i = V_a - k_v \omega_m$$

Solving for k_v yields

$$k_v = \frac{V_a - R_a i}{\omega_m}$$

With a known input voltage, the armature was measured with a current probe while the rotational velocity was measured with a tachometer. Using the tachometer required conversion from RPM to rad/s which was done by multiplying the RPM reading by $\pi/30$. A low speed and a high speed trial was observed to verify k_v as a constant.

	V_a [V] <i>Digital Multimeter</i>	i_a [A] <i>Current Probe</i>	ω_m [RPM] <i>Tachometer</i>	ω_m [rad/s] <i>[rad/s]=RPM*π/30</i>
Trial 1:	20.50	0.95	270	28.274
Trial 2:	50.45	1.04	735	76.969

Table 2. Voltage and Current Measurements at Low and High Speed

For these trials, it was appropriate use $R_a = 3.2 [\Omega]$ for the calculation based on $i = 1.0 [A]$ in Table 1. This yielded

$$k_{v1} = \frac{20.5 - (3.2)(0.95)}{28.274} = 0.6175 \text{ [V/rad/s]}$$

$$k_{v2} = \frac{50.45 - (3.2)(1.04)}{76.969} = 0.6122 \text{ [V/rad/s]}$$

These values are relatively equivalent, so an average k_v was computed. The k_v and k_T used in future calculations are:

$$k_v = 0.615 \text{ [V/rad/s]}$$

$$k_T = 0.615 \text{ [N m/A]}$$

It should be noted that the previous two determinations were performed with no load wheel attached. Armature inductance and resistance do not vary with rotor load.

Determination of Motor Viscous Friction Coefficient and Coloumbic Friction Torque Constant

For the next experiments, the wheel has been reattached. The viscous friction coefficient and coloumbic friction torque constant have to be found concurrently. When the wheel is rotated at an unchanging velocity ($\frac{d\omega_m}{dt} = 0$), Equation (14) simplifies:

$$0 = k_T i - B\omega_m - T_{cf}$$

With k_T known, two trials can be measured as done in the previous determination to yield two independent equations.

	i [A] <i>Current Probe</i>	ω_m [RPM] <i>Tachometer</i>	ω_m [rad/s] <i>[rad/s]=RPM*π/30</i>
Trial 1:	1.038	200	20.93
Trial 2:	1.350	735	76.93

Table 3. Current and Rotational Velocity Measurements at Low and High Speed

These trials resulted in the following independent equations:

$$\text{Trial 1: } 0 = (0.615)(1.038) - B(20.94) - T_{cf}$$

$$\text{Trial 2: } 0 = (0.615)(1.350) - B(52.36) - T_{cf}$$

Solving the system of equations yields $B=0.0061$ [N m/(rad/s)] and $T_{cf}=0.5105$ [N m].

Determination of Moment of Inertia

Solving the differential equation in (14) for rotational velocity ω_m yields the following relationship:

$$\omega_m(t) = \left[\omega_m(0^+) + \frac{T_{cf}}{B} \right] e^{-\left(\frac{B}{J}\right)t} - \frac{T_{cf}}{B} \quad [\text{rad/s}] \quad (15)$$

A Coast Down Test can be performed by rotating the rotor at a constant rotational velocity $\omega_m(0^+)$, then observing the Back emf Voltage V_b as it varies with time. Equation (15) can be translated by using the Back emf Voltage – Rotational Velocity relationship in (13):

$$V_b(t) = k_v \left[\left[\omega_m(0^+) + \frac{T_{cf}}{B} \right] e^{-\left(\frac{B}{J}\right)t} - \frac{T_{cf}}{B} \right] \quad [\text{Volts}] \quad (16)$$

When observing the transient response of the motor on an oscilloscope, any voltage at time t can be used in (16). To be thorough, two transients were observed, one at high speed and one at low speed, and two data points were taken from each transient.

	$\omega(0^+) [\text{RPM}]$ <i>Tachometer</i>	$\omega(0^+) [\text{rad/s}]$ <i>[rad/s]=[RPM]*$\pi/30$</i>	t [sec]	$V_b(t) [\text{V}]$ <i>Voltage Probe</i>
Trial 1:	498	52.15	0.20	26.0
			0.80	8.6
Trial 2:	1010	105.77	0.40	52.6
			1.50	18.0

Table 4. Transient Response Measurements at Low and High Speed

Using Table (4), four separate calculations were made for the Moment of Inertia.

$$J_{11} = 0.2471 [\text{kg m}^2]$$

$$J_{12} = 0.2920 [\text{kg m}^2]$$

$$J_{21} = 0.2413 [\text{kg m}^2]$$

$$J_{22} = 0.2603 [\text{kg m}^2]$$

An average Moment of Inertia was used $J=0.261 [\text{kg m}^2]$.

Motor Model Accuracy

In order to test these parameters, the steady state response and the transient response will be compared with the motor's experimental results. In order to test the responses, The motor's system block diagram will be simulated. Shown in Figure (13) is the motor's system block diagram with the parameter measurements.

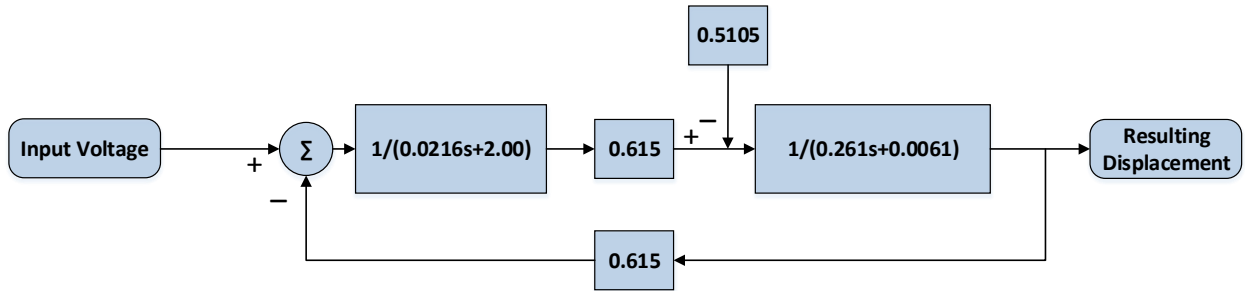


Fig. 13. Motor Model Subsystem – Experimentally determined

With this block diagram, simulations can be analyzed in SIMULINK. However, before analysis, experimental results will have to be derived to compare with the simulations. Shown in Table (5), is experimentally measured steady state response rotational velocity measuring for a range of input voltages.

Voltage		Velocity	
V_a (V)	F_{enc} (Hz)	v_{RPM} (rpm)	ω_m (rad/s)
7.15	5.600	84.000	8.792
8.32	6.800	102.000	10.676
9.76	8.100	121.500	12.717
11.15	9.500	142.500	14.915
13.00	11.300	169.500	17.741
14.65	12.800	192.000	20.096
16.85	15.200	228.000	23.864
20.34	19.000	285.000	29.830
24.95	23.800	357.000	37.366
30.29	28.700	430.500	45.059
35.71	34.500	517.500	54.165
40.60	39.900	598.500	62.643
45.35	45.000	675.000	70.650
49.96	49.000	735.000	76.930
54.86	54.750	821.250	85.958

59.92	60.000	900.000	94.200
64.70	65.000	975.000	102.050

Table 5. Experimental Steady State Velocities Results

In this experiment, an optical encoder was used in lieu of a tachometer to improve the accuracy of resulting velocity. The optical encoder output 4 pulses/revolution. Its frequency shown in the second column can be converted into RPM shown in the third column by multiplying frequency by 15:

$$RPM = 60 \frac{\text{seconds}}{\text{minute}} / 4 \frac{\text{pulses}}{\text{revolution}}$$

Similarly, radians per second shown in the fourth column can be calculated with the following conversion:

$$\text{radians/second} = 2\pi \frac{\text{radians}}{\text{revolution}} / 60 \frac{\text{seconds}}{\text{minute}}$$

With an experimental relationship between input voltage and output rotational velocity recorded, simulations were performed at the same input voltages.

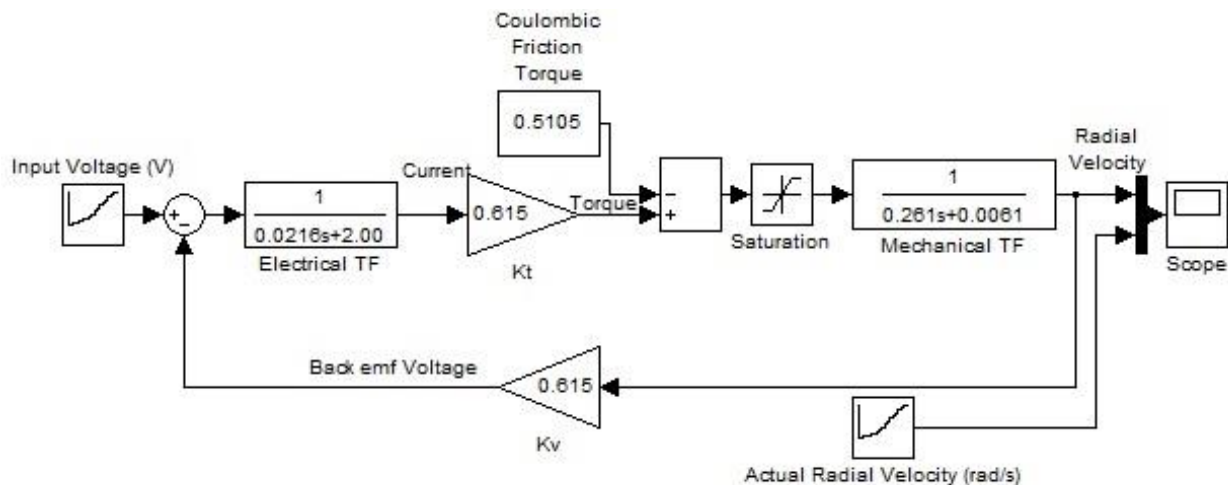


Fig. 14. Motor Model Subsystem – SIMULINK Diagram

Figure (14) shows the SIMLINK diagram representation of the motor model. For the simulation, Input Voltage shown on the left of the diagram was set to output all 17 voltages from Table (5), column 1,

changing every 10 seconds to allow the simulation to reach steady state. For comparison, Actual Radial Velocity shown at the bottom right of the diagram was set to the resulting radial velocities from Table (5), column 4. Figure (15) displays the resulting output of the Scope in the diagram.

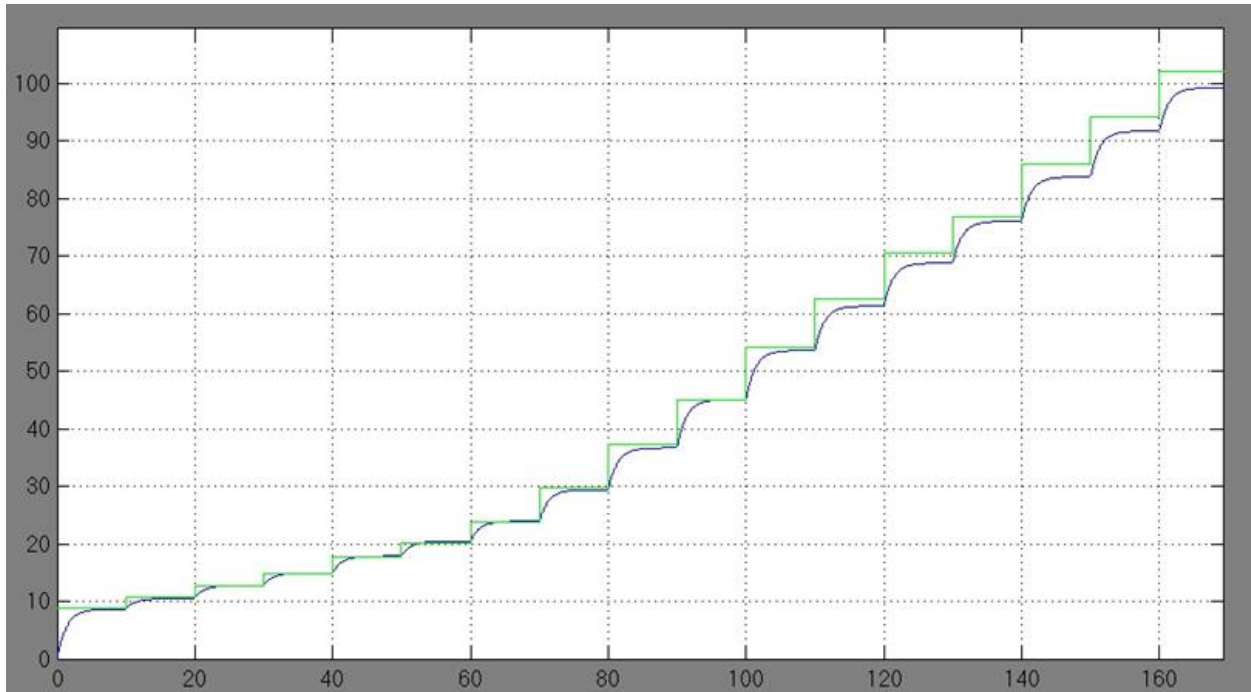


Fig. 15. SIMULINK Output – Comparison of Simulation Radial Velocity (blue) and Actual Radial Velocity (green)

While analyzing the results of the simulation, it was noted that the model performs relatively well when predicting steady state velocity. It was also noted that gap between the simulation and the actual radial velocity increases as voltage increases. A more thorough error analysis was performed on the steady state results.

Voltage	Velocity	SIMULINK Model	% Error
V_a (V)	ω_m (rad/s)	ω_m (rad/s)	
7.15	8.792	8.643	-1.69%
8.32	10.676	10.490	-1.75%
9.76	12.717	12.758	0.32%
11.15	14.915	14.947	0.22%
13.00	17.741	17.861	0.68%
14.65	20.096	20.460	1.81%
16.85	23.864	23.925	0.26%
20.34	29.830	29.421	-1.37%

24.95	37.366	36.682	-1.83%
30.29	45.059	45.092	0.07%
35.71	54.165	53.630	-0.99%
40.60	62.643	61.333	-2.09%
45.35	70.650	68.815	-2.60%
49.96	76.930	76.077	-1.11%
54.86	85.958	83.795	-2.52%
59.92	94.200	91.765	-2.58%
64.70	102.050	99.295	-2.70%

Table 6. Experimental Steady State Velocities Comparative Analysis

Table (6) uses the same input voltage and radial velocities experimentally measured in Table (5). Added to the table in column 3 is the SIMULINK model steady state values exported from MATLAB. The fourth column is the calculated Error percentage between Actual Radial Velocity and Modeled Radial Velocity. Column 4 shows that error percentage never surpasses 3%. It was concluded that our model accurately predicts rotational velocity within 3% from approximately 8.5 – 100 rad/s or about 100 – 1000 RPM.

The previous motor model analysis reveals steady state accuracy. However, we were also able to analyze the transient response of the model. The experimental transient response of the motor was recorded as in the Determination of Moment of Inertia experiment.

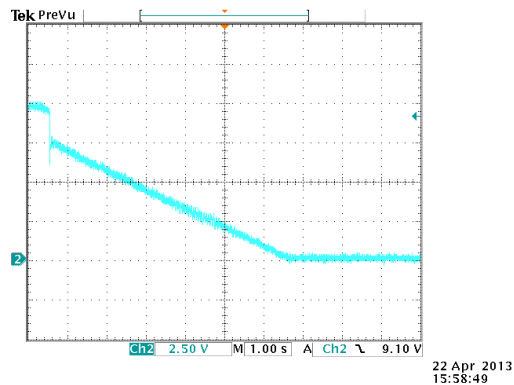


Fig. 16. Transient Response - $V_a = 9.65 \text{ V}$ $w_{ss} = 12.4 \text{ rad/s}$

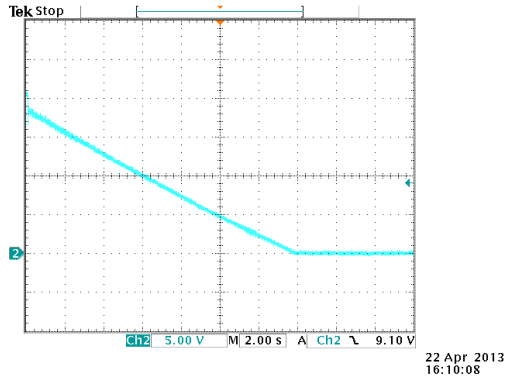


Fig. 27. Transient Response - $V_a = 20.6 \text{ V}$ $\omega_{ss} = 29.4 \text{ rad/s}$

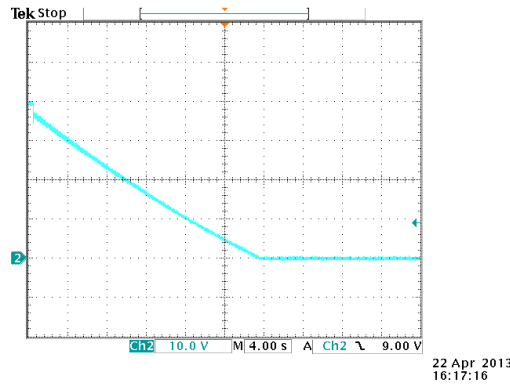


Fig. 38. Transient Response - $V_a = 39.5 \text{ V}$ $\omega_{ss} = 59.7 \text{ rad/s}$

The voltage was recorded from the oscilloscope every second and a plot was created in Excel. For comparison, the motor model's simulation of the transient response was calculated and overlaid. The model's prediction is calculated by Equation (16)

$$V_b(t) = k_v \left[\left[\omega_m(0^+) + \frac{T_{cf}}{B} \right] e^{-\left(\frac{B}{J}\right)t} - \frac{T_{cf}}{B} \right] \quad [\text{Volts}] \quad (16)$$

With the derived parameters,

$$V_b(t) = 0.615 \left[\left[\omega_m(0^+) + \frac{0.5105}{0.0061} \right] e^{-\left(\frac{0.0061}{0.261}\right)t} - \frac{0.5105}{0.} \right] \quad [\text{Volts}]$$

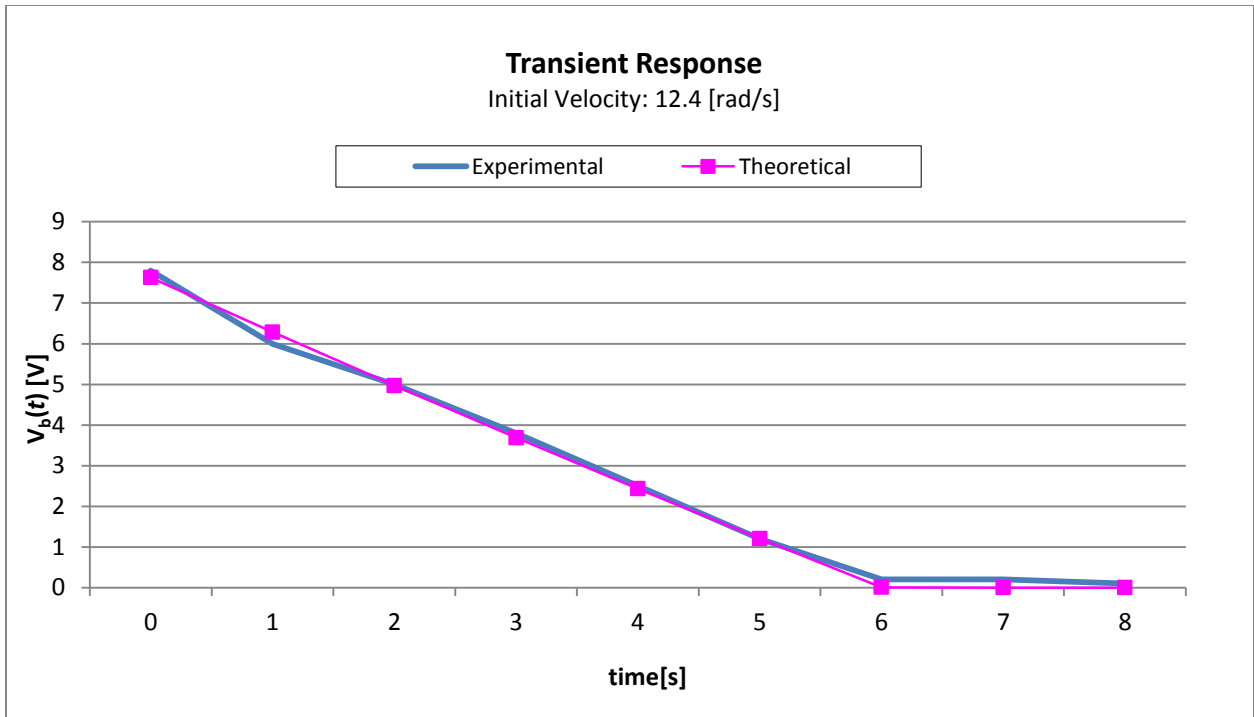


Fig. 49. Transient Response – Experimental vs Theoretical (12.4 rad/s)

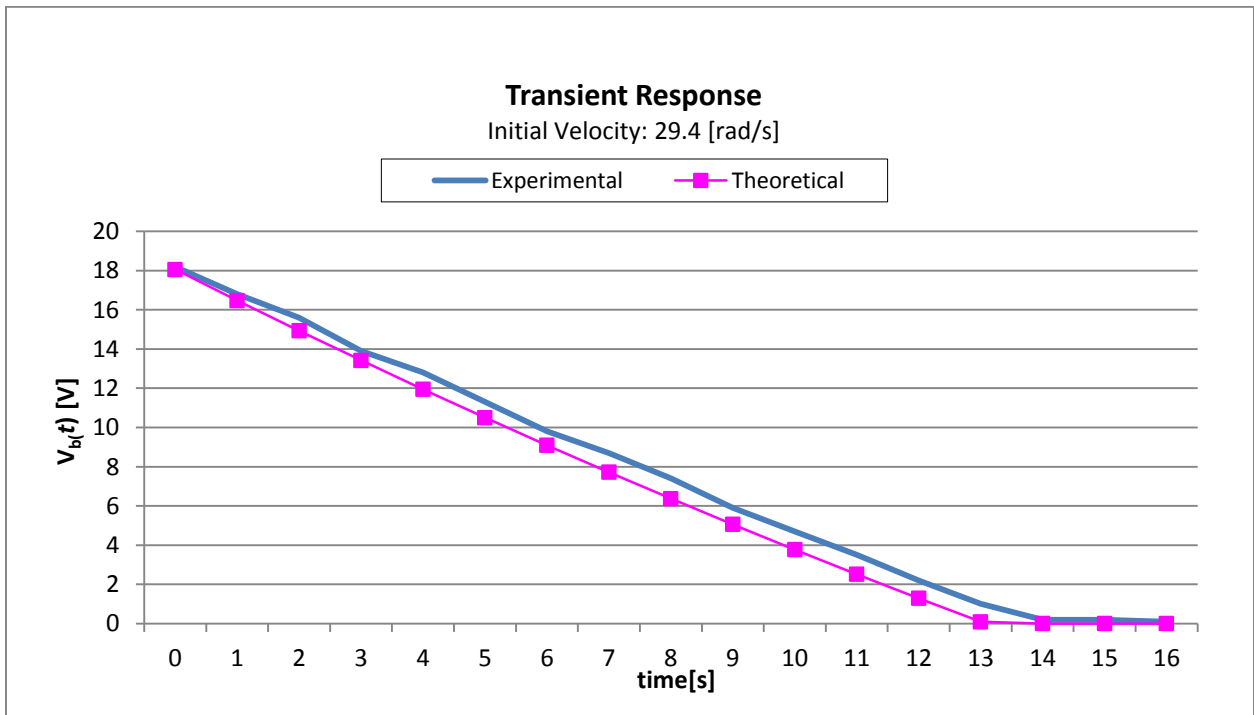


Fig. 20. Transient Response – Experimental vs Theoretical (29.4 rad/s)

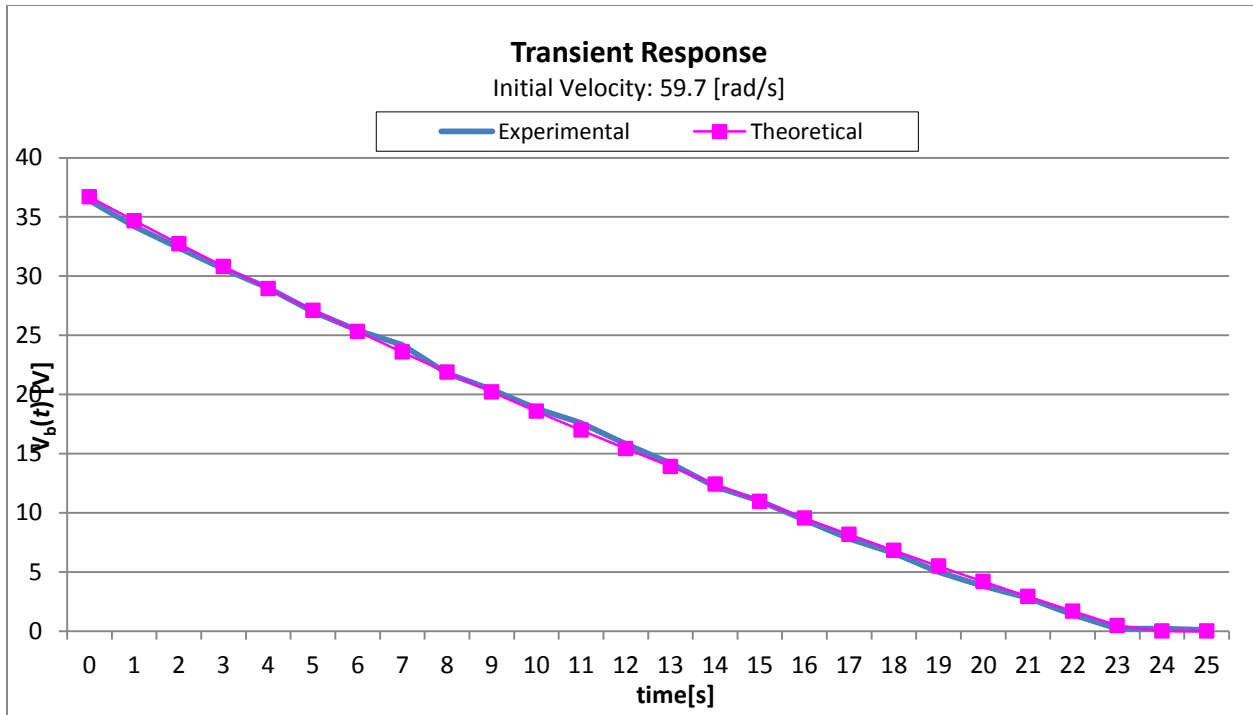


Fig. 21. Transient Response – Experimental vs Theoretical (59.7 rad/s)

The transient analysis show that the experimental data correlates well with the motor model’s calculated response. Analysis of the motor model’s transient and steady state response show the model performing to a highly acceptable level.

Controller Design

With the model made, we design a controller based on the motor model to the specifications outlined earlier. First, an analysis of the motor’s poles and zeroes is needed. Using system block diagram reduction of the motor model yields the following transfer function:

$$G(s) = 109.09 \frac{1}{s^2 + 92.62s + 69.25} \quad (17)$$

This transfer function has two poles, one at -91.86 rad/s and another at -0.75 rad/s. Figure (22) shows a pole zero map of the open loop transfer function.

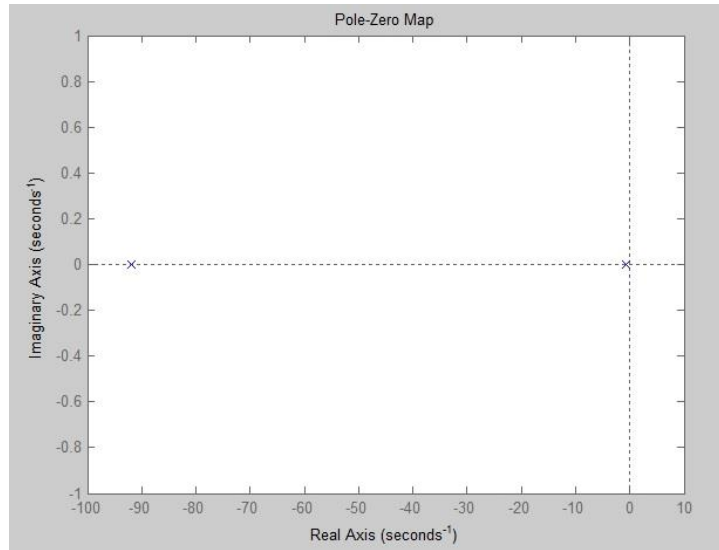


Fig. 22. Pole Zero Map of Open Loop Motor Model

Design Specifications

We broke down each specification into its meaning for the controller.

Specification 1: Steady State error shall be zero for unit step input.

Interpretation: The controller will have an integrator.

Specification 2: Overshoot shall be less than 10%

Interpretation: We will design the controller with closed loop poles so that damping ratio will equal 0.707. Shown in Figure (23) is the $\zeta = 0.707$ line.

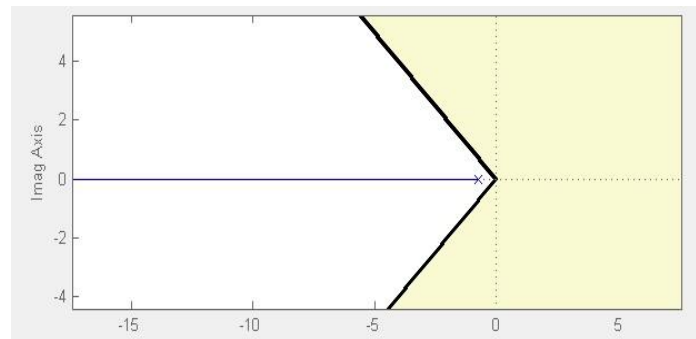


Fig. 23. Root Locus with Damping Ratio

Specification 3: Settling time shall be less than 4 seconds

Interpretation: We will design the controller with closed loop poles so that settling time equals 4 seconds. Shown in Figure () is the $t_s = 4$ seconds line along with the damping ratio line. The pink box represents where the closed loop poles shall be.

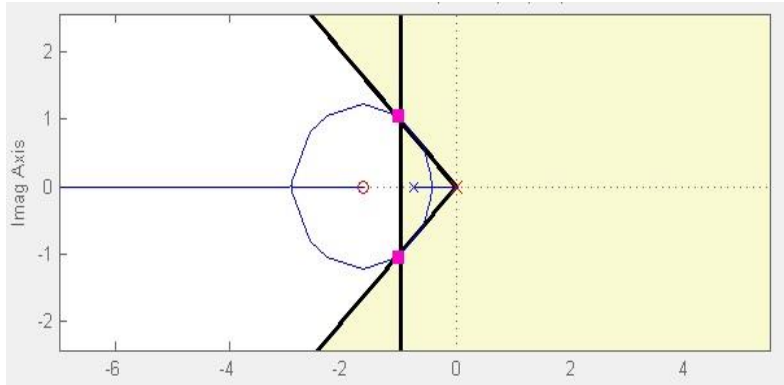


Fig. 24. Root Locus with Damping Ratio and Settling Time

Design Method

Root locus theory was used to design the controller shown previously. The SISO tool in MATLAB allowed for dynamic pole and zero placement. The following transfer function was derived to meet the design specifications discussed previously.

$$C(s) = 75.71 \frac{s+1.56}{s(s+76.92)} \quad (18)$$

Controlled Motor Model Response

The controller is simulated using SIMULINK. The block diagram is shown below:

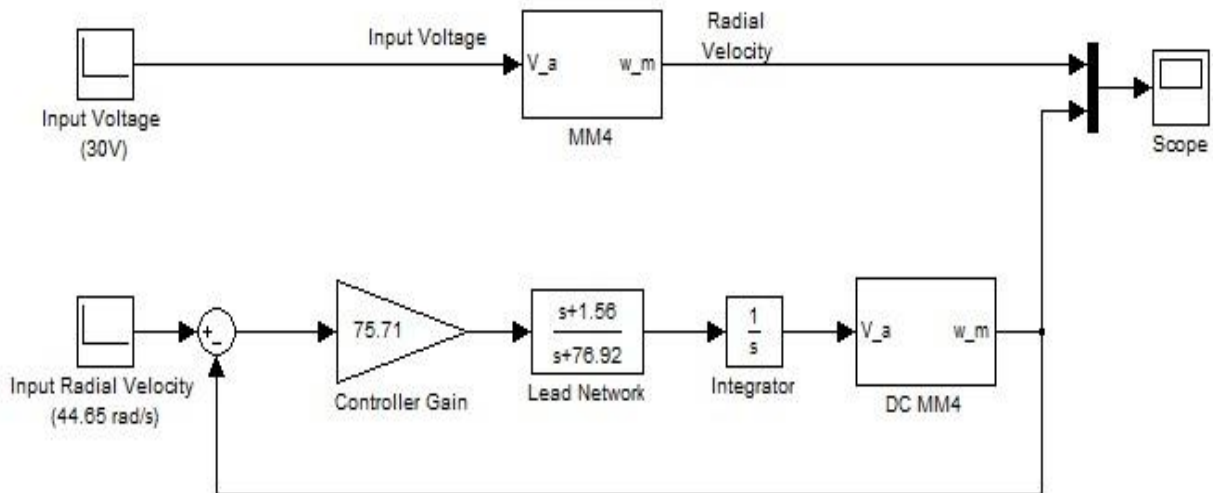


Fig. 25. Controller SIMULINK Block Diagram

The corresponding plot comparing the uncontrolled motor with the controlled motor is shown in Figure (26).

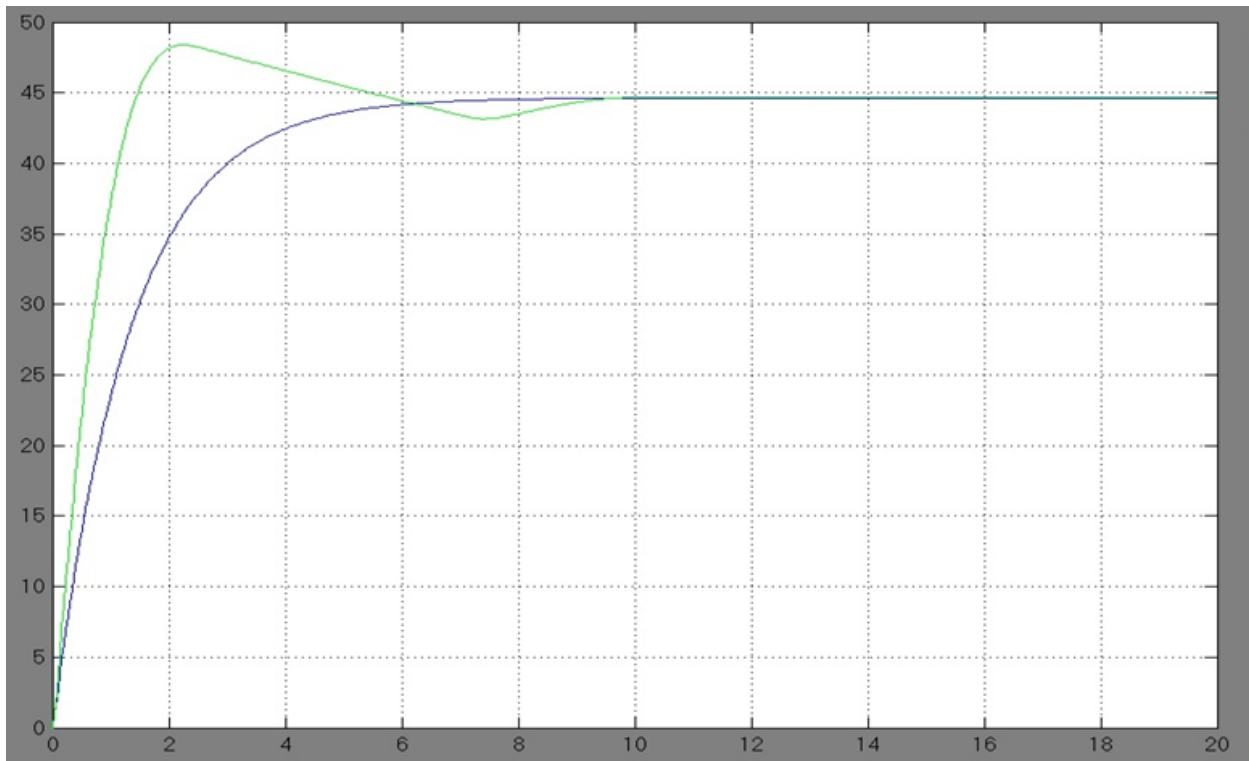


Fig. 25. Controller SIMULINK Block Diagram

This plot allows us to see that the peak rotational velocity is 48.41 rad/s, which represents an 8.4% overshoot. Additionally, we see that the uncontrolled motor comes within 5% of its steady state speed at approximately 4 seconds, while the controlled motor reaches this same range in ~3.6 seconds. Finally, there is no steady state error in the controlled motor. This allows us to confirm that the controller which has been designed meets all 3 major design specifications.

Digital Controller

The continuous time controller can be converted to a discrete time controller using the “C2D” function in MATLAB. The sampling time is determined to be 0.01s based on the bandwidth of the closed loop system. The discrete controller can be written as:

$$C(z) = \frac{0.5453 - 0.5369z^{-1}}{1 - 1.463z^{-1} + 0.4634z^{-2}} \quad (19)$$

This transfer function will be re-written in the form of a difference equation to allow implementation on the microcontroller.

$$y(k) - 1.463 y(k - 1) - 0.4634 y(k - 2) = 0.5453 x(k) - 0.5369 x(k - 1) \quad (20)$$

Halbach Array Data Collection

The lookup table was created by taking data comparing the displacement data with the rotational velocity. Force data was also taken to confirm theoretical expectations of the force generated by the system.

Displacement Sensor Data

The displacement sensor is placed directly above the Halbach array and allows us to measure the vertical displacement experienced by the system. This sensor provides a voltage which can be converted to a displacement. This data is collected in table form and displayed below. This data will be used to generate the lookup table on the microcontroller.

Measured Data					Theoretical Data	
Input Voltage	Displacement Sensor Voltage	Encoder Frequency	Velocity	Height	Electrical Frequency	Height
Va [V]	[V]	Fenc [Hz]	ω m [rad/s]	y [mm]	ω e [rad/s]	y [mm]
4.72	3.73	2.10	3.30	7.00	169.21	-0.81
9.39	3.73	5.60	8.80	7.01	451.24	3.52
10.25	3.72	6.20	9.74	7.08	499.59	3.96
11.20	3.71	6.90	10.84	7.18	555.99	4.43
12.18	3.71	7.50	11.78	7.25	604.34	4.79
13.13	3.70	8.40	13.19	7.35	676.86	5.27
14.12	3.69	9.10	14.29	7.45	733.26	5.61
15.07	3.67	9.80	15.39	7.57	789.67	5.92
17.06	3.66	11.70	18.38	7.69	942.77	6.65
18.92	3.64	13.10	20.58	7.87	1055.58	7.11
21.08	3.61	15.00	23.56	8.21	1208.68	7.64
23.08	3.60	16.60	26.08	8.37	1337.60	8.03
25.03	3.58	18.50	29.06	8.56	1490.70	8.43
30.12	3.47	25.00	39.27	9.61	2014.46	9.45
35.21	3.42	31.00	48.69	10.17	2497.93	10.07
40.32	3.37	36.00	56.55	10.69	2900.82	10.45
45.36	3.34	42.00	65.97	10.97	3384.29	10.79
50.40	3.31	47.00	73.83	11.26	3787.18	11.00
55.40	3.29	52.00	81.68	11.49	4190.08	11.17
60.35	3.28	57.00	89.54	11.62	4592.97	11.31
65.54	3.26	63.00	98.96	11.76	5076.44	11.44
70.50	3.25	68.00	106.81	11.92	5479.33	11.53
75.38	3.24	73.00	114.67	12.01	5882.22	11.60
80.33	3.23	79.00	124.09	12.14	6365.69	11.67
85.53	3.21	84.00	131.95	12.28	6768.58	11.72
90.92	3.21	90.00	141.37	12.37	7252.06	11.77
95.61	3.20	95.00	149.23	12.46	7654.95	11.81
100.50	3.19	100.00	157.08	12.57	8057.84	11.84
105.50	3.17	105.00	164.93	12.69	8460.73	11.86
110.00	3.17	110.00	172.79	12.77	8863.62	11.89

Table 7. Displacement Sensor Data Collection with Theoretical Results

This data is plotted in Figure (26) to compare the experimental results with the theoretical expectation.

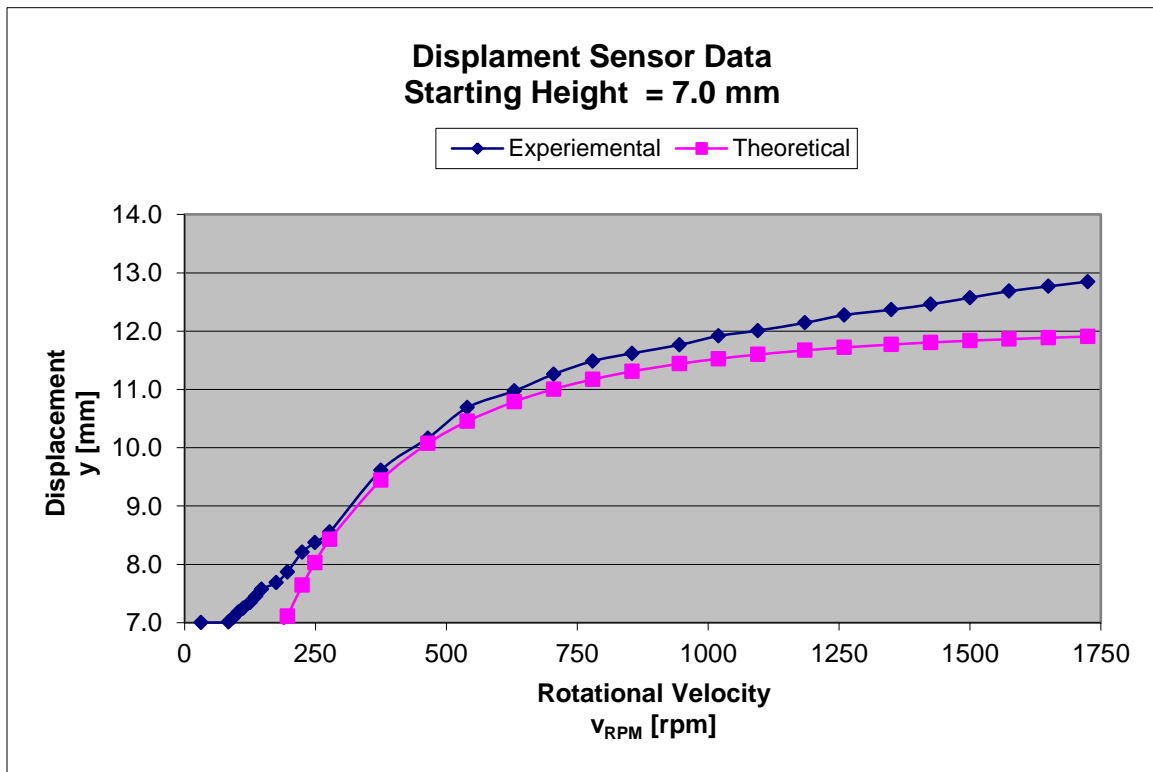


Fig. 26. Experimental Displacement vs. Theoretical Displacement

Analyzing this comparison we can see that the Halbach array experienced some vertical force before reaching the breakpoint velocity. This is a result of the instability of the Halbach array and the effects of the drag force. As the rotational velocity increases along with the displacement height, the experimental data presents a displacement which is larger than expected theoretically. This is believed to be the result of some vibration, as well as the nonlinear nature of the displacement conversion coefficient. In future work the coefficient used to convert the displacement sensor voltage to a displacement would need to be dynamic based on the height of the array.

Force Sensor Data

In place of the displacement sensor, a force sensor is installed which restricts the vertical displacement of the Halbach array. By holding the Halbach array stationary we are able to measure the total vertical force it experiences. As a result of the Halbach array remaining at the initial displacement height much larger torques are experienced, resulting in currents which must be monitored to avoid damaging the motor. The initial force sensor data was found to be incorrect, but the plot will be displayed below for analysis.

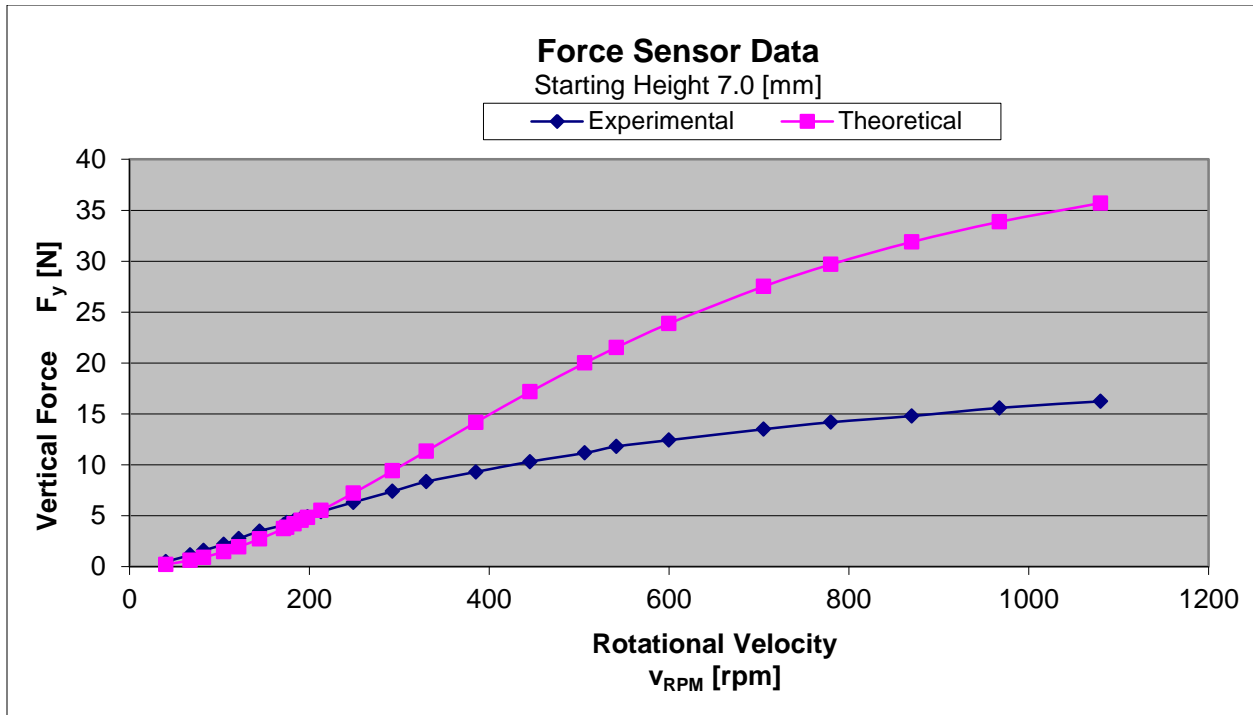


Fig. 27. Force Sensor Data before Mounting Improvements

This plot allows us to see the inaccuracies of this initial set of data. Early values provide reasonable results, while increased speeds provide forces much lower than expected. The current measurements aid us in determining that the force sensor was not secured properly and was allowed vertical motion. This resulted in the Halbach array's vertical displacement to increase and resulted in reduced current values. The system was revisited and method used to mount the force sensor was improved dramatically. The data recorded after this improvement is shown in Table 8.

Measured Data					Theoretical Data	
Current	Voltage	Force	Encoder Frequency	Velocity	Electrical Frequency	Force
I_a [A]	V_a [V]	F_y [N]	F_{enc} [Hz]	ω_m [rad/s]	ω_e [rad/s]	F_y [N]
0.00	0.00	0.00	0.00	0.00	0.00	0.00
1.36	5.00	0.55	2.70	4.24	217.45	0.14
2.12	9.71	1.56	6.36	9.99	512.22	0.78
2.92	14.63	3.00	10.13	15.90	815.85	1.91
3.60	19.32	4.60	14.00	21.98	1127.53	3.44
4.20	24.00	6.00	18.00	28.26	1449.68	5.28
4.80	29.18	7.80	22.47	35.28	1809.68	7.47
5.40	34.48	9.30	27.80	43.65	2238.95	10.08
5.76	40.36	10.90	32.50	51.03	2617.47	12.23
6.00	45.90	12.20	38.30	60.13	3084.59	14.61
6.20	51.30	13.23	43.26	67.92	3484.06	16.38
6.28	58.58	14.65	50.80	79.76	4091.31	18.64

6.36	63.98	15.50	57.30	89.96	4614.80	20.21
6.40	69.38	16.45	62.70	98.44	5049.71	21.30
6.40	74.37	17.18	66.77	104.83	5377.50	22.00
6.40	79.81	17.94	73.80	115.87	5943.68	23.04
6.44	85.08	18.65	79.00	124.03	6362.47	23.68
6.52	89.43	19.40	83.56	131.19	6729.72	24.17
6.48	95.55	20.16	89.63	140.72	7218.59	24.74

Table 8. Force Sensor Data Collection with System Improvements

We see in this set of data that the current remains similar across the values collected. This provides us increased confidence that the improvements to the mounting method were successful in mitigating the vertical movement of the force sensor and Halbach array. In addition to these mounting improvements, the initial displacement height was increased from 7.0 mm to 8.0 mm to reduce the maximum amount of force generated. This was done to assist in improving data measured using the force sensor.

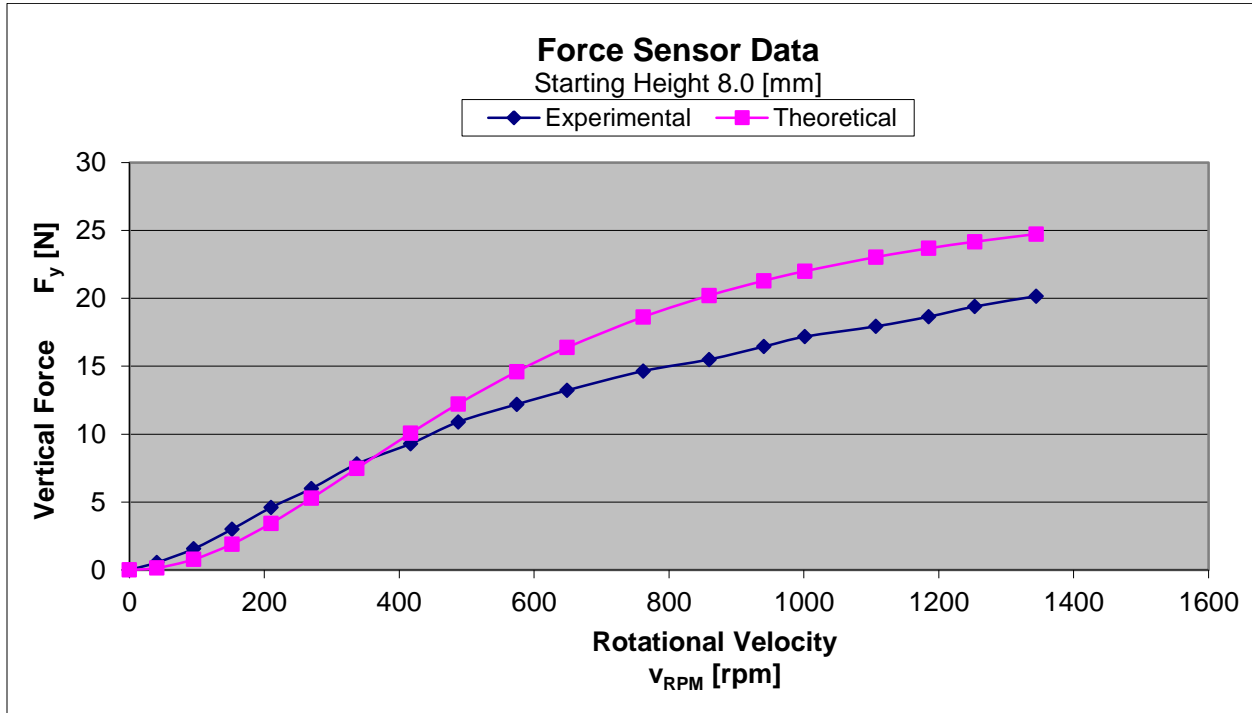


Fig. 28. Force Sensor Data with Mounting Improvements

This new set of data correlates similarly at low speeds, and continues to provide reasonable data as the rotational velocity increases. In addition to the changes made to the mounting of the force sensor, we also took steps to increase the stability of the mounting of Halbach array itself. With this goal in mind the aluminum cross piece suspending the Halbach array was replaced with a similar piece of steel. This increased strength reduced the twist experienced by the Halbach array resulting from the drag force at high rotational velocities.

Microcontroller Implementation

We chose to use the emac board due to our familiarity with it from previous courses. Additionally, the projects worked on in Junior Lab were helpful in providing us a foundation on which we could build. Some of the systems designed will be discussed below, but the final implementation was not completed. The completed portions of the microcontroller system include: user input, PWM signal output, mock lookup table, RPM display. The tachometer portion of this project was used with a Pittman motor to test its function. While working properly on a Pittman motor, it requires significant redesign for use with the maglev system. The PWM signals are generated properly by the microcontroller, but require a power MOSFET to drive the motor. This circuitry has been designed, built, and tested with the Pittman motor, but requires additional testing with the maglev system. Finally, the lookup table is currently designed with dummy variables to allow for variable duty cycles for testing purposes. The displacement sensor data taken previously will need to be used to determine the necessary rotational velocity, and a corresponding duty cycle value will need to replace these dummy variable in the lookup table.

Results

The initial objectives of this project were as follows:

- Improve the rotational stability of the inductrack by balancing the wheel
- Construct a safety enclosure in order to safely reach higher rotational velocities
- Model the DC motor and verify its accuracy to within +/- 5% of steady state rotational velocity
- Design a controller to achieve closed loop control of displacement height
- Implement the controller using a microcontroller

The work we have completed during the last two semesters allowed us to complete a majority of these objectives, but did not enable us to implement the microcontroller portion. By working with JH Benedict we were able to bring the wheel to within 2g of balance. The services provided by JH Benedict were a key component to reaching the high speeds we achieved. The safety enclosure has been constructed and provides observers a hazard free environment.

The motor model exceeded the specifications by providing a steady state accuracy within +/- 3% up to 1000 RPM. Additionally the transient response was shown to correlate with the experimental results. This motor model can be used with high levels of confidence in any further work on this project.

The controller which we have designed has been tested in both the continuous time domain as well as the discrete time domain. By modeling this controller in Simulink and simulating the motor model,

continuous time controller, and discrete time controller on the same plot we are able to confirm that validity of this controller and its uses.

Unfortunately, the microcontroller portion of our project was not able to be completed before the end of the semester. This is partially due to difficulties encountered in other aspects of the project, but also due to the limitations we found with the emac board. With better research we could have seen these limitations in advance and avoided them by using a more suitable microcontroller. For future work on this project we would advise that groups explore other microcontroller options.

Patents

Richard F. Post
Magnetic Levitation System for Moving Objects
U.S. Patent 5,722,326
March 3, 1998

Richard F. Post
Inductrack Magnet Configuration
U.S. Patent 6,633,217 B2
October 14, 2003

Richard F. Post
Inductrack Configuration
U.S. Patent 6,295,503 B2
October 7, 2003

Richard F. Post
Laminated Track Design for Inductrack Maglev
System
U.S. Patent Pending US 2003/0112105 A1
June 19, 2003

Coffey; Howard T.
Propulsion and stabilization for magnetically
levitated vehicles
U.S. Patent 5,222,436
June 29, 2003

Coffey; Howard T.
Magnetic Levitation configuration incorporating
levitation, guidance and linear synchronous
motor
U.S. Patent 5,253,592
October 19, 1993

Levi; Enrico; Zabar; Zivan
Air cored, linear induction motor for
magnetically levitated systems
U.S. Patent 5,270,593
November 10, 1992

References

- [1] Dirk DeDecker, Jesse VanIseghem. Senior Project. "Development of a Halback Array Magnetic Levitation System". Final Report, May 2012
- [2] Glenn Zomchek. Senior Project. "Redesign of a Rotary Inductrack for Magnetic Levitation Train Demonstration." Final Report, 2007.
- [3] Paul Friend. Senior Project. Magnetic Levitation Technology 1. Final Report, 2004.
- [4] Post, Richard F., Ryutov, Dmitri D., "The Inductrack Approach to Magnetic Levitation," Lawrence Livermore National Laboratory.
- [5] Post, Richard F., Ryutov, Dmitri D., "The Inductrack: A Simpler Approach to Magnetic Levitation," Lawrence Livermore National Laboratory.
- [6] Post, Richard F., Sam Gurol, and Bob Baldi. "The General Atomics Low Speed Urban Maglev Technology Development Program." Lawrence Livermore National Laboratory and General Atomics.